

Sparse Discrete Fractional Fourier Transform and Its Applications

Shengheng Liu, *Student Member, IEEE*, Tao Shan, Ran Tao, *Senior Member, IEEE*, Yimin D. Zhang, *Senior Member, IEEE*, Guo Zhang, Feng Zhang, *Member, IEEE*, and Yue Wang

Abstract—The discrete fractional Fourier transform is a powerful signal processing tool with broad applications for nonstationary signals. In this paper, we propose a sparse discrete fractional Fourier transform (SDFrFT) algorithm to reduce the computational complexity when dealing with large data sets that are sparsely represented in the fractional Fourier domain. The proposed technique achieves multicomponent resolution in addition to its low computational complexity and robustness against noise. In addition, we apply the SDFrFT to the synchronization of high dynamic direct-sequence spread-spectrum signals. Furthermore, a sparse fractional cross ambiguity function (SFrCAF) is developed, and the application of SFrCAF to a passive coherent location system is presented. The experiment results confirm that the proposed approach can substantially reduce the computation complexity without degrading the precision.

Index Terms—Cross ambiguity function, global positioning system, passive bistatic radar, sparse discrete fractional Fourier transform.

I. INTRODUCTION

THE discrete fractional Fourier transform (DFrFT) is a generalization of the discrete Fourier transform (DFT) with an additional free order parameter [1], which requires a much higher computational complexity than the DFT. Similar to the fast Fourier transform (FFT) [2] that promoted the applications of DFT, an efficient computation method is also needed to facilitate the applications of DFrFT.

A number of definitions and fast computational algorithms of DFrFT have been derived in recent years. Among them, the most common types include the eigenvector decomposition type [3]–[5], the linear combination type [6] and the sampling type [7]–[9]. However, the eigenvector decomposition based approach cannot be expressed in a closed form, and the run-time is $O(N^2)$ for an N -point data set, while the transformed

results of the linear combination type do not match those of the continuous fractional Fourier transform (FrFT). In contrast, the sampling based approach has a closed form expression with a relatively low complexity of $O(N \log_2 N)$, and the transformed results approach that of the continuous FrFT [9]. Therefore, the sampling based DFrFT is widely employed in engineering applications.

Among the various types of DFrFT algorithms, the lowest complexity is achieved by the Pei's algorithm [9]. The Pei's algorithm can be further optimized via a novel sub-linear algorithm for DFT named sparse Fourier transform (SFT) developed by Haitham *et al.* [10], [11]. When the input data have a large size with a sparse spectrum, this algorithm reduces the complexity of DFT to $O(\log_2 N \cdot \sqrt{kN \log_2 N})$, where k stands for the number of large coefficients in the frequency domain. Consider a wideband chirp signal with a sparse feature in the fractional Fourier domain, to accelerate the time-frequency analysis of such signals, we propose an efficient scheme through redesigning Pei's algorithm by exploiting the advantage of the SFT framework.

In addition to the SFT algorithm, pruning [12] is also a frequently referred approach to implement DFT by exploiting signal sparsity. Unlike SFT, however, the sparsity pattern of the signal has to be known in advance when using pruning. Another difference between the two algorithms is that the SFT is a probabilistic algorithm while the pruning FFT algorithm is deterministic.

In our previous related works, we investigated the spectral analysis and reconstruction in the fractional Fourier domain [13], the fractional power spectrum [14], the sampling theorems in the fractional Fourier domain [15], [16], time delay estimation of chirp signals in the fractional Fourier domain [17], and the short-time FrFT [18]. On this basis, we propose the sparse discrete fractional Fourier transform (SDFrFT) to achieve fast computation of DFrFT in this paper.

Many challenging engineering applications can be formulated as large-scale signal analysis problems in the fractional Fourier domain. Therefore, the proposed algorithm can benefit the applications in spectrum sensing, radio astronomy, radar signal processing, digital medical imaging, communication, cryptography and compression [19], [20]. Due to the limited space, we only select two applications in this paper to illustrate the effectiveness of the proposed algorithm: acquisition of high dynamic direct-sequence spread-spectrum (DSSS) signals used in the global positioning system (GPS) and coherent integration of accelerating targets in passive coherent location (PCL) systems.

Manuscript received June 06, 2014; revised August 22, 2014; accepted October 08, 2014. Date of publication October 31, 2014; date of current version November 14, 2014. The associate editor coordinating the review of this manuscript and approving it for publication was Prof. Antonio Napolitano. This research was supported in part by the National Natural Science Foundation of China under Grant No. 61421001, 61331021, 61172176 and 61201354. (Corresponding authors: T. Shan and R. Tao.)

S. Liu, T. Shan, R. Tao, G. Zhang, F. Zhang, and Y. Wang are with the School of Information and Electronics, Beijing Institute of Technology and the Beijing Key Laboratory of Fractional Signals and Systems, Beijing 100081, China (e-mail: shantao@bit.edu.cn; rantao@bit.edu.cn).

Y. D. Zhang is with the Center for Advanced Communications, Villanova University, Villanova, PA 19085 USA.

Color versions of one or more of the figures in this paper are available online at <http://ieeexplore.ieee.org>.

Digital Object Identifier 10.1109/TSP.2014.2366719

The contribution of this paper is fivefold: (1) We propose the concept and algorithm of SDFrFT; (2) We analyze its important properties such as the capability of resolving multiple signal components; (3) We apply the SDFrFT to the fast synchronization of high dynamic GPS signals; (4) We develop sparse fractional cross ambiguity function (SFrCAF) to reduce the computational complexity of radar signal processing; (5) We apply the proposed SFrCAF to a PCL system to yield desirable results.

The rest of the paper is arranged as follows. In Section II, the proposed SDFrFT algorithm is presented, and its relationship with the Pei's algorithm and the SFT is discussed. Simulation results and performance analysis of the proposed algorithm are given in Section III. In Section IV, we apply the SFrCAF to the fast acquisition of high dynamic DSSS signals. In Section V, the principle of the proposed SFrCAF and its application to the PCL signal processing is demonstrated. The paper is concluded in Section VI.

II. METHODOLOGY

A. SDFrFT Algorithm

1) *Algorithm Flow*: From a practice perspective, the computational efficiency of an algorithm is a critical factor. The main steps of the proposed SDFrFT algorithm are as follows:

Step 1) Construct the input signal of the SFT stage from the original input signal $f(n)$ by a chirp multiplication. Note that $f(n)$ must be sparse in fractional Fourier domain and nonperiodic, and satisfy the Dirichlet condition.

$$x(n) = f(n) \cdot e^{\frac{j}{2} \cot \alpha n^2 \Delta t^2}, \quad n \in [1, N], \quad (1)$$

where Δt is the sampling interval of the input signal, α is a real number representing the rotation angle of FrFT.

Step 2) To tear apart the nearby coefficients in the spectrum, a permutation is adopted to reorder the signal's frequency domain $X(n)$. This process is conducted by modifying the time-domain signal $x(n)$ as we do not have access to the input signal's Fourier spectrum, which would require performing a DFT [21]. We permute the constructed signal $x(n)$ as follows:

$$s(n) = x((\sigma \cdot n) \bmod N), \quad n \in [1, N], \quad (2)$$

where $\sigma \in [1, N]$ is a random odd number that is invertible mod N , and mod denotes the modulo operation that finds the remainder of division of one number by another: Given two positive numbers a and b , $a \bmod b$ yields the remainder of the Euclidean division of a by b . Assume that

$$\exists \sigma^{-1} \text{ s.t. } (\sigma \times \sigma^{-1}) \bmod N = 1, \quad (3)$$

so that the relation between the frequency domain representations of $s(n)$ and $x(n)$ is [10]

$$S(m) = X((\sigma^{-1} \cdot m) \bmod N), \quad m \in [1, N]. \quad (4)$$

Step 3) To extract parts of a signal in a smooth way and avoid spectral leakage, a window function is used

[21]. Define a flat window function $g(n)$, which is a symmetric vector, $n \in [1, N]$. Let w denote the window length in the time domain. Suppose that $G(m)$ is the frequency domain expression of $g(n)$, whose range obeys

$$G(m) \in \begin{cases} [1 - \delta, 1 + \delta], & m \in [-\varepsilon'N, \varepsilon'N], \\ [0, \delta], & m \notin [-\varepsilon N, \varepsilon N], \end{cases} \quad (5)$$

where ε' and ε are the truncation factors of the passband and stopband, respectively, and δ denotes the extent of ripple oscillation. Define a signal $y(n) = g(n) \cdot s(n)$, $n \in [1, N]$, then the support of $y(n)$ satisfies $\text{supp}(y) \subseteq \text{supp}(g) = [-\frac{w}{2}, \frac{w}{2}]$.

Step 4) Let N be an exact divisor of integer B . If $\sin \alpha > 0$, construct a signal

$$\begin{aligned} Z(m) &= \text{FFT} \{z(n)\} \\ &= \text{FFT} \left\{ \sum_{i=0}^{\lfloor \frac{w}{B} \rfloor - 1} y(n + i \cdot B) \right\}, \quad n \in [1, B]. \end{aligned} \quad (6)$$

On the other hand, if $\sin \alpha < 0$, substitute the FFT operation with IFFT. Assume that $Y(m)$ is the frequency domain expression of signal $y(n)$. It can be proved that [10], [29]

$$Z(m) = Y(m \cdot N/B), \quad m \in [1, B]. \quad (7)$$

(7) indicates that aliasing in the time domain corresponds to subsampling in the frequency domain. Store the value of $Z(m)$ and parameter σ employed in (2).

Step 5) Define a hash function

$$h_\sigma(m) = \lfloor \sigma \cdot m \cdot B/N \rfloor, \quad (8)$$

and an offset function

$$o_\sigma(m) = \sigma \cdot m - h_\sigma(m) \cdot N/B. \quad (9)$$

Step 6) Location loops: Define another set

$$\mathcal{J} = \arg \max_m |Z(m)|, \quad (10)$$

where \mathcal{J} contains the $2k$ coordinates of the maximum magnitudes in $Z(m)$. Output the preimage

$$\mathcal{I} = \{m \in [1, N] \mid h_\sigma(m) \in \mathcal{J}\}. \quad (11)$$

The size of \mathcal{I} is $2kN/B$.

Step 7) Estimation loops: We can estimate the k largest coefficients of $X(m)$ as follows:

$$\hat{X}(m) = \begin{cases} \frac{Z(h_\sigma(m)) e^{-j\pi o_\sigma(m) w/N}}{G(o_\sigma(m))}, & m \in \mathcal{I}, \\ 0, & m \in [1, N] \cap \bar{\mathcal{I}}. \end{cases} \quad (12)$$

Let l be the number of loops, l_{loc} and l_{est} be two positive integers, and $l_{\text{total}} = l_{\text{loc}} + l_{\text{est}}$. For $l \leq l_{\text{loc}}$, execute the steps between *Step 2–Step 6*. For $l_{\text{loc}} < l \leq l_{\text{total}}$, execute the steps between *Step 2–Step 7*. The process is terminated when $l > l_{\text{total}}$. It can be seen that the location loops are actually executed for

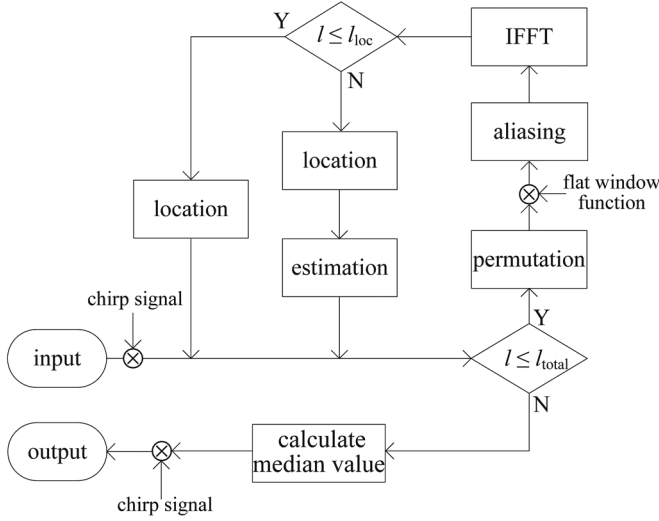


Fig. 1. Architecture for SDFrFT algorithm when $\sin \alpha < 0$.

l_{total} times, and the estimation loops are executed for l_{est} times.

Step 8) The estimated output of $X(m)$ can be obtained by selecting the median values of the real and the imaginary parts separately:

$$\tilde{X}(m) = \text{Median}_{l_{\text{est}}} \left\{ \text{Re} \left\{ \hat{X}(m) \right\} \right\} + j \cdot \text{Median}_{l_{\text{est}}} \left\{ \text{Im} \left\{ \hat{X}(m) \right\} \right\}. \quad (13)$$

Step 9) By multiplying another chirp function to the estimation result $\tilde{X}(m)$ obtained from the above steps, the output of the SDFrFT algorithm is finally given by

$$\hat{F}_\alpha(m) = \tilde{X}(m) \cdot e^{\frac{j m^2 \Delta u^2}{2 \tan \alpha}} \sqrt{(\sin \alpha - j \cos \alpha) \cdot \text{sgn}(\sin \alpha) / M}, \quad (14)$$

where Δu is the sampling interval of the output signal, and M is the length of the DFrFT output. The detailed overall computation architecture for the $\sin \alpha < 0$ situation is presented in Fig. 1.

2) *Selection of α* : With regard to the selection of the value of α , there are two cases in practice:

Case 1) The value of α is already known. This kind of situation exists in many applications, for example, the matched filtering in the linear frequency modulation radar or in the synthetic aperture radar (SAR) imaging.

Case 2) The value of α is unknown. For this case, we estimate the value of α by the discrete polynomial-phase transform (DPT) method [22], [23]. The estimation precision can be further improved by searching with a finer step size within a limited range around the estimated value of α .

We explain how to choose the value of α as follows.

An important method to estimate the rotation angle α is the maximum likelihood estimation (MLE) technique [24]. In [25], the discrete chirp Fourier transform, which is the discrete form of the MLE, is proposed to estimate the chirp rate. However, due to the exhausting two-dimensional maximization process of the MLE, suboptimal methods are preferred. The phase unwrapping method [26] is developed based on the finite difference operator,

but it appears incapable of analyzing multicomponent signals. As a computationally efficient alternative to the MLE method, the DPT with order 2 converts the chirp signal into a sinusoidal wave [23]. In this way, the rotation angles of the multicomponent signals can be quickly determined.

In our work, we adopt the DPT-based approach to estimate the rotation angle α . Let $x(n)$ be a complex-valued function of a real discrete variable n , and τ be a positive integer representing delay parameter. The operators $\mathcal{DP}_1[x(n), \tau]$ and $\mathcal{DP}_2[x(n), \tau]$ are defined as

$$\mathcal{DP}_1[x(n), \tau] \triangleq x(n), \quad (15)$$

$$\mathcal{DP}_2[x(n), \tau] \triangleq x(n)x^*(n - \tau), \quad (16)$$

where $*$ denotes conjugate operation. We also introduce an operator \mathcal{DPT} , which is the DFT of \mathcal{DP} . Note that \mathcal{DP}_2 performs phase differencing, and it can be proved that differencing reduces the order of the polynomial by one.

Consider a signal $s(n) = x(n) \exp\{j\pi\mu(n\Delta t)^2\}$, where Δt represents the sampling interval, and μ is the chirp rate. We get

$$\begin{aligned} \mathcal{DPT}_2[x(n)e^{j\pi\mu(n\Delta t)^2}, \omega, \tau] &= \text{DFT} \left\{ \mathcal{DP}_2[x(n)e^{j\pi\mu(n\Delta t)^2}, \tau] \right\} \\ &= \text{DFT} \left\{ e^{j2\pi\mu\tau n(\Delta t)^2 - j\pi\mu(\tau\Delta t)^2} \right\}. \end{aligned} \quad (17)$$

According to (17), the energy of $\mathcal{DPT}_2[x(n)e^{j\pi\mu(n\Delta t)^2}, \omega, \tau]$ will concentrate at

$$\omega = \omega_0 = 2\pi\mu\tau\Delta t, \quad (18)$$

and it is proved that the best estimation precision can be obtained with $\tau = \frac{N}{2}$. Then, α can be correctly estimated from μ .

However, influenced by the input channel noise, the estimation precision may not be sufficient for some application scenarios. For these cases, a fine search for the value of α within a limited range around the estimated result is required. In the process, the selection of the step size $\Delta\alpha$ mainly depends on the chirp rate resolution and application requirement. Here we derive the upper bound of $\Delta\alpha$ under the constraint of chirp rate resolution $\Delta\mu$. From (18) we know that

$$f = \mu\tau\Delta t \Rightarrow \Delta f = \Delta\mu\tau\Delta t. \quad (19)$$

Let T be the time length of the signal, and choose $\tau = \frac{N}{2}$. Then we can get

$$\Delta\mu = \frac{\Delta f}{\tau\Delta t} = \frac{\frac{2}{T}}{\frac{T}{2}} = \frac{4}{T^2}. \quad (20)$$

Comparing (1) with (17), we can find that

$$\frac{\cot \alpha}{2} = \pi\mu \Rightarrow (\cot \alpha)' \Delta\alpha = 2\pi\Delta\mu \Rightarrow |\Delta\alpha| = \frac{8\pi \sin^2 \alpha}{T^2}, \quad (21)$$

where $(\cdot)'$ denotes first-order derivative operator.

B. Relation to the Pei's Sampling-Type Algorithm and the Concept of SFT

The continuous FrFT [27] is defined as (22), at the bottom of the page, where u denotes the fractional Fourier domain frequency, D is an integer, $\alpha = p\pi/2$, and the phase of $\sqrt{1 - j \cot \alpha}$ is constrained in the range of $(-\pi/4, \pi/4)$.

The Pei's sampling-type algorithm [9] is derived based on (22). First, the input and the output signals are directly sampled by the intervals Δt and Δu , respectively. Second, to satisfy the reversible property, the sampling interval is restricted by

$$\Delta t \cdot \Delta u = \frac{2\pi |\sin \alpha|}{M}. \quad (23)$$

Denote the length of input signal by N . Then, the constraint $M \geq N$ must be satisfied. We only discuss the $M = N$ situation in this paper. In this case, the form of DFrFT can be obtained as shown in (24) at the bottom of the page.

Generally, if $\alpha \neq D\pi$, the Pei's sampling-type algorithm can be seen as two times of multiplication with chirp signals and one time of FFT. Therefore, the overall multiplication complexity of the Pei's algorithm is $O(2N + \frac{N}{2} \log_2 N)$.

As the most efficient numerical algorithm of DFrFT, the Pei's sampling-type algorithm is suited for a broad spectrum of applications. However, the computational complexity will be high when the data length N is large, in which the FFT stage accounts for a major proportion. When the signal is sparse, i.e., most of its coefficients are zero or negligible, it is recently revealed that the computational complexity of DFT can be significantly reduced by a novel fast algorithm named SFT [10], which is far superior to the FFT. The key idea of SFT is to first partition the frequency domain of the sparse signal into individual buckets using a specially designed filter that is concentrated both in time and frequency domains, which is obtained by convolving a Dolph-Chebyshev function with a box-car function,

then locate and estimate the large coefficients in a manner similar to the sketching/streaming algorithms, where either iteration or interpolation, the expensive process in the previous methods, is needed. This makes it possible for further improvement of the algorithm efficiency on the basis of the Pei's sampling-type algorithm. Fortunately, it happens that the algorithm architecture of the Pei's algorithm is suited for this kind of modification.

The revised Pei's algorithm, termed SDFrFT, is designed for the signals that meet the following descriptions: The signal is non-stationary with a large scale, and is k -sparse in the fractional Fourier domain, where the signal size N and the number of large coefficients k satisfy $k \ll N$. This kind of signal is common in many applications, such as SAR signal processing and nuclear magnetic resonance imaging.

III. PERFORMANCE OF PROPOSED SDFrFT

A. Resolution Performance

In the following an example is given to illustrate the resolution performance of the proposed SDFrFT in the multi-rotation angle case. The initial frequencies of the four frequency components are 100, 200, 300 and 300.1 Hz, respectively, and the chirp rates of these components are 10, 11.85, 13.85 and 13.85 Hz/s, respectively. The sampling rate is $f_s = 900$ Hz, and the data length is $N = 2^{15}$. The input signal is corrupted by a white Gaussian noise, and the SNRs of the four frequency components are -12 , -18 , -24 and -24 dB, respectively. In the simulation process, the number of computed large coefficients in the frequency domain is set to $k = 5$. The loop number parameters are set as $l_{\text{loc}} = 4$ and $l_{\text{est}} = 15$, respectively. The filter parameters are set as $w = 22883$, $\delta = 10^{-6}$, $\epsilon' = 2 \times 10^{-4}$, and $\epsilon = 5 \times 10^{-4}$. The length of subsampled FFT is $B = 2048$. In every location loop, as many as $2k = 10$ maximum magnitudes are searched out from Z .

$$\begin{aligned} \{\mathcal{F}^\alpha x\}(u) &= \int_{-\infty}^{\infty} K_\alpha(u, t)x(t)dt, \quad 0 < |p| < 2, 0 < |\alpha| < \pi \\ &= \begin{cases} \sqrt{\frac{1-j \cot \alpha}{2\pi}} \int_{-\infty}^{\infty} e^{j\frac{t^2+u^2}{2} \cot \alpha - jtu \csc \alpha} \cdot x(t)dt, & \alpha \neq D\pi, \\ x(t), & \alpha = 2D\pi, \\ x(-t), & \alpha = (2D \pm 1)\pi, \end{cases} \end{aligned} \quad (22)$$

$$\{\mathcal{F}^\alpha x\}(m) = \begin{cases} \sqrt{\frac{\sin \alpha - j \cos \alpha}{M}} e^{\frac{jm^2 \Delta u^2}{2 \tan \alpha}} \sum_{n=0}^{N-1} x(n) e^{\frac{j}{2} \cot \alpha n^2 \Delta t^2} e^{-\frac{j2\pi nm}{M}}, & \alpha \in 2D\pi + (0, \pi), \\ \sqrt{\frac{-\sin \alpha + j \cos \alpha}{M}} e^{\frac{jm^2 \Delta u^2}{2 \tan \alpha}} \sum_{n=0}^{N-1} x(n) e^{\frac{j}{2} \cot \alpha n^2 \Delta t^2} e^{\frac{j2\pi nm}{M}}, & \alpha \in 2D\pi + (-\pi, 0), \\ x(m), & \alpha = 2D\pi, \\ x(-m), & \alpha = (2D + 1)\pi. \end{cases} \quad (24)$$

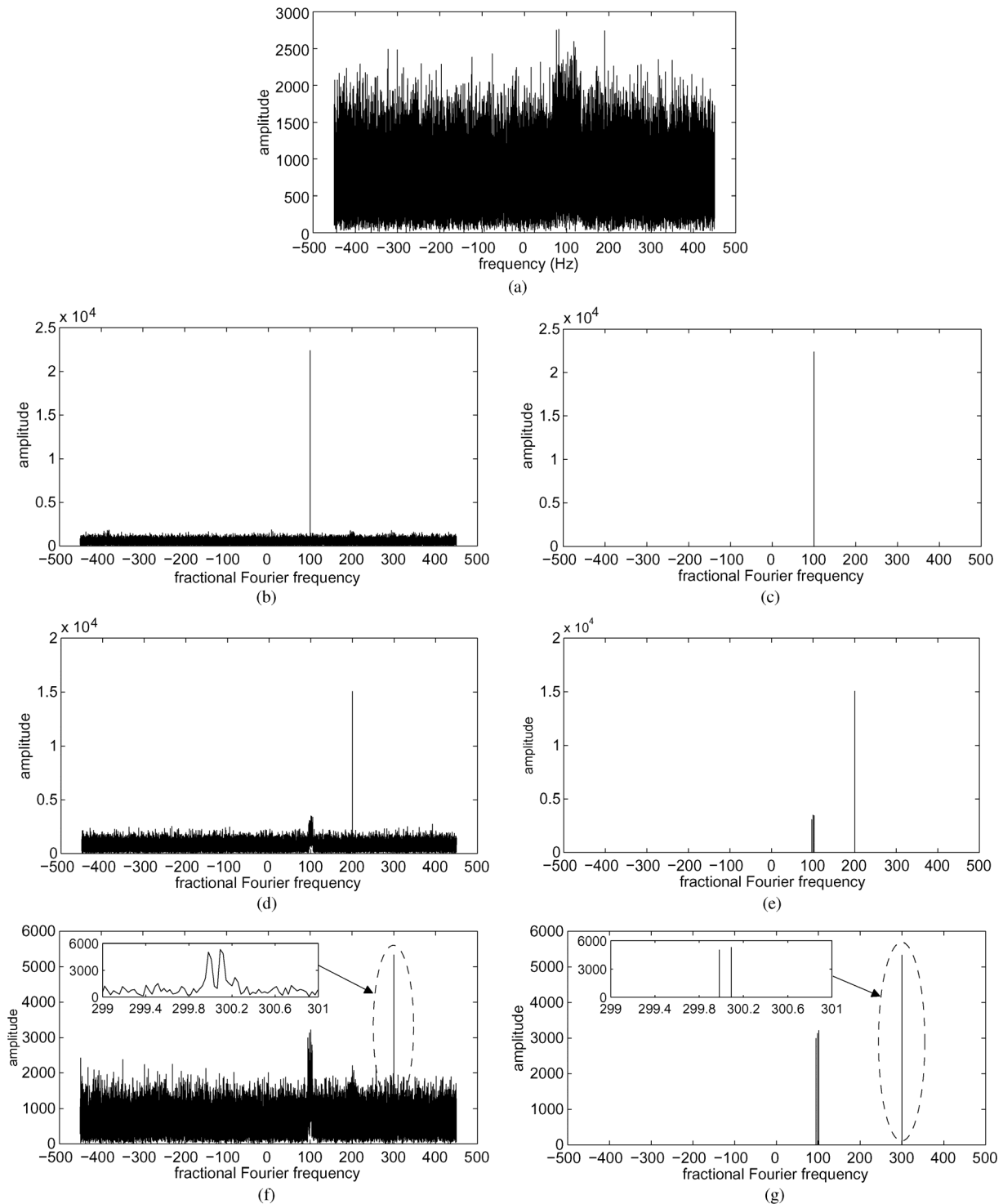


Fig. 2. The resolution performance of SDFrFT: (a) The frequency domain of the input signal. (b) (d) (f) The matched-order DFrFT of the four components respectively. (c) (e) (g) The matched-order SDFrFT of the four components, respectively.

The simulation results are shown in Fig. 2, where Fig. 2(a) shows the frequency domain magnitude of the input signal, and the rest are arranged in 3 rows and 2 columns. The results in each row are obtained by setting the rotation angle α in the fractional Fourier domain such that one of the frequency components is focused. The simulation results demonstrate that, in this multi-rotation angle case, the estimation precision of the fractional frequency and the amplitude value of the

sparse component in the fractional Fourier domain can be guaranteed by the proposed SDFrFT. On the other hand, in the estimated fractional Fourier domain, the components which do not behave sparse and focused will be estimated as dense fractional spectral lines with lower amplitude as compared with the correctly estimated large values. The enlargements in Figs. 2(f) and (g) reveal the local details of the immediately adjacent spectral lines with the same chirp

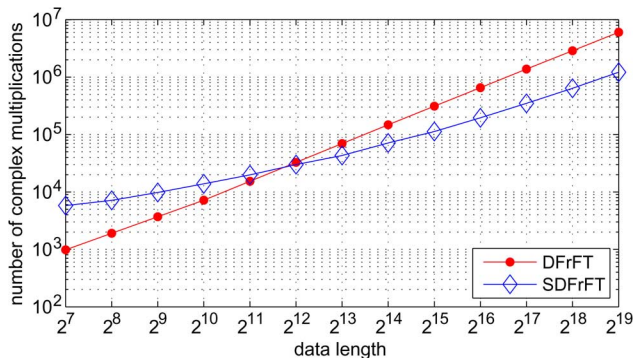


Fig. 3. Comparison of the computational complexity between conventional DFrFT and SDFrFT approaches.

rate, indicating that the SDFrFT processing does not affect the resolution performance.

B. Computational Complexity

The calculation of the proposed SDFrFT involves a total number of

$$\#M_{\text{SDFrFT}} = 2N + (w + B \cdot \log_2 B/2 + 2 \cdot k) \times l_{\text{loc}} + (w + B \cdot \log_2 B/2) \times l_{\text{est}} + \text{card}(\mathcal{I}) \times l_{\text{total}} \quad (25)$$

complex multiplication operations, where the function $\text{card}(\cdot)$ expresses the cardinality of a set.

The comparative result of the computation complexity between SDFrFT and DFrFT is shown in Fig. 3. Note that the result is simply based on the number of complex multiplications in the unoptimized algorithm flow as depicted in (25). In the simulation process, we assume the number of computed large coefficients in the frequency domain to be $k = 5$. The loop number parameters are set as $l_{\text{loc}} = 3$ and $l_{\text{est}} = 8$, respectively. It can be seen that, when the data length is increased to a moderate level, the advantage of the SDFrFT over the DFrFT in computational complexity becomes more evident.

The proposed SDFrFT algorithm is designed based on the SFT theory [10] and code versions 1 and 2 [28]. As is pointed out in [21], the computational complexity of these two versions closely correlates with the signal size N . The version 3 and 4 codes are not published yet. However, the theories of these two versions have been described in [29], and some analysis of version 3 can be found in [21]. It is proved that, in code version 3, the correlation between signal size and computational complexity becomes less significant. Thus it is reasonable to expect that the SDFrFT based on SFT code version 3 will not necessarily require such a large signal size to exceed the classic algorithm.

On the other hand, our algorithm is already computationally faster for signals with length around 2^{12} , which is a quite common size in many application scenarios. Some of the examples will be presented in Section IV and Section V.

C. Algorithm Robustness

As illustrated in [10], the SFT's reduced runtime does not compromise its robustness to noise. The robustness to noise of the proposed algorithm is examined by simulations. Let $N =$

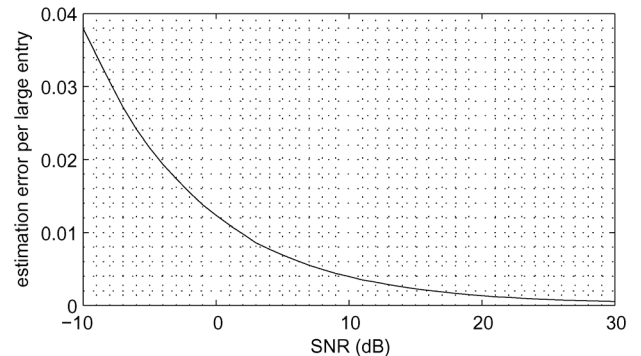


Fig. 4. Robustness vs. SNR.

2^{15} , $k = 3$, and $\alpha = 0.01$ rad. 20000 Monte Carlo trials are conducted with different SNRs ranging from -10 dB to 30 dB. For each trial, we compute the average value of the estimation error per large entry between the SDFrFT output $\{S\mathcal{F}^\alpha x\}(i)$ and the best k -sparse approximation of the DFrFT output $\{\mathcal{F}^\alpha x\}(i)$, which can be expressed as

$$\mathcal{E} = \frac{1}{k} \sum_{i \in (0, N]} \left| \frac{\{S\mathcal{F}^\alpha x\}(i) - \{\mathcal{F}^\alpha x\}(i)}{\{\mathcal{F}^\alpha x\}(i)} \right|. \quad (26)$$

Fig. 4 plots the average error of the SDFrFT obtained from the numeric simulation results, which confirms the robustness of the algorithm under noisy circumstance.

IV. APPLICATION TO THE SYNCHRONIZATION OF HIGH DYNAMIC DSSS SIGNAL

DSSS communication and navigation systems [30] have the advantages of low spectral density, high information security and resistance to jamming, and are easy to realize multiple access communications and high-precision measurements. Hence, they are widely used in both civilian and military applications. The well-known GPS [31] is an example of DSSS system. To ensure correct despreading and demodulation, signal synchronization is needed at the receiver end. The synchronization in a DSSS system normally consists of two steps: acquisition and tracking, where acquisition is the prerequisite for tracking. GPS receivers are now frequently used in the field of aerospace engineering. The commonly occurring high dynamic relative motion between the navigation satellite and the receiver platform will induce acute variations in the phase of the carrier. The high velocity and acceleration of the motion are characterized as a large Doppler shift and its derivative.

Conventional FFT based fast acquisition approaches [32]–[34] solely compensate for the Doppler shift component caused by the high velocity, whereas the impact of the change rate of the Doppler frequency is ignored. However, if the change rate of the Doppler frequency is high, then the spectral expansion results in a reduction of the signal peak, and thereby, makes the acquisition difficult, especially with an extremely low SNR. In this section, we propose a fast acquisition method based on the SDFrFT to synchronize high dynamic DSSS signals. By compensating the quadratic phase term with SDFrFT, a notably enhanced acquisition performance can be achieved.

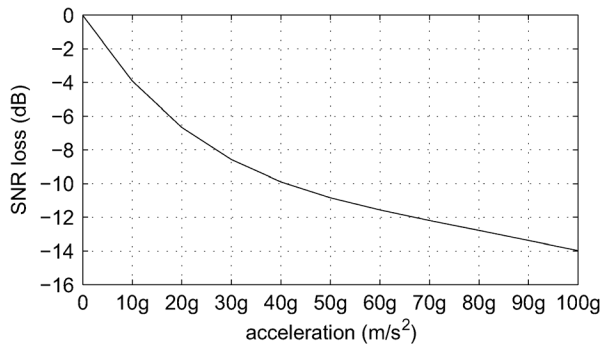


Fig. 5. The relationship between integration loss and dynamic strain.

A. Principle

Let v_0 and a be the initial velocity and acceleration of the receiver platform relative to the transmitter respectively. Let λ denote the carrier wavelength, so the Doppler frequency f_d at time t can be written as

$$f_d(t) = \frac{v_0 + at}{\lambda}. \quad (27)$$

Thus, the received signal can be expressed as

$$\begin{aligned} s_i(t) &= d(t)c(t) \cos \left(2\pi \left(f_I t + \int_0^t f_d(\tau) d\tau \right) \right) \\ &= d(t)c(t) \cos \left(2\pi \left(f_I + \frac{v_0}{\lambda} \right) t + \frac{\pi a}{\lambda} t^2 \right), \end{aligned} \quad (28)$$

where $d(t)$ and $c(t)$ represent the modulated data code and spread spectrum code, respectively, and f_I denotes the intermediate frequency (IF). It can be seen from (28) that the relative accelerating motion of the receiver platform will bring in a quadratic phase term to the modulated signal, which will directly influence the acquisition performance. Take GPS receiver for instance. When FFT is adopted to process the received signal, the impact of acceleration on the signal peak is shown in Fig. 5, where the wavelength is 0.1904 m, the sampling rate is 5 MHz, and the integration time is 0.08 s. It can be concluded from Fig. 5 that the amplitude of the signal peak declines with the increase of the acceleration. The loss of signal peak is about 4 dB when the acceleration is 10 g, whilst the loss reaches 10 dB when the acceleration is 40 g, where $g \approx 9.8 \text{ m/s}^2$ represents the gravity acceleration.

The fastest GPS synchronization algorithm is presented in [34], where SFT is exploited to reduce the computational complexity. For real GPS signals, the results in [34] show that the new algorithm reduces the median number of multiplications by a factor of 2.2 in comparison to the FFT-based synchronization algorithm. Based on this method, a SDFrFT based synchronization algorithm is proposed to deal with the high dynamic situation as shown in Fig. 6.

It is emphasized that the synchronization output has a single major peak at the correct rotation angle and time delay, while the FrFT of the input signal is not sparse. Therefore, in the inverse FrFT step, the proposed SDFrFT can be adopted to lower the runtime. Since the function of the front FrFT step is to provide the input for the inverse FrFT step, and the SDFrFT step needs only few samples of the FrFT output, a subsampled DFrFT is

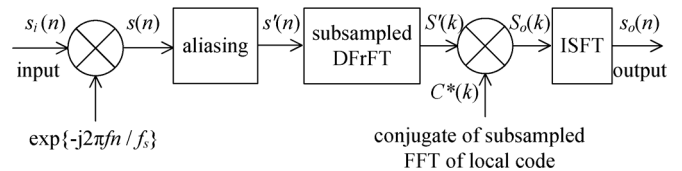


Fig. 6. The architecture of the SDFrFT based synchronization algorithm.

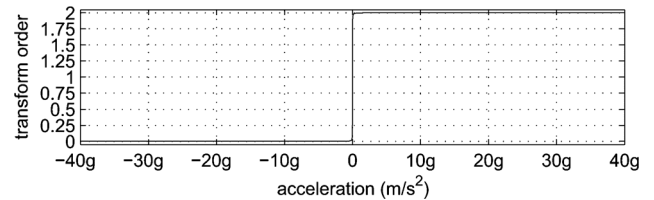


Fig. 7. The relationship between acceleration and transform order.

adopted to further reduce the computational complexity. When searching for the Doppler frequency \hat{f}_{d0} , the input signal $s_i(n)$ is first multiplied by $e^{-j2\pi f n / f_s}$ to obtain $s(n)$, where $f = f_I + \hat{f}_{d0}$. As subsampling a signal in the frequency domain is equivalent to aliasing it in the time domain, and vice versa, signal $s(n)$ is aliased to obtain its subsampled version $s'(n)$ as

$$s'(n) = \sum_{i=0}^{L/N-1} s(n + i \cdot N), \quad n \in [1, N], \quad (29)$$

where L is the number of samples. The output is divided into N buckets with L/N samples in each bucket. Then a subsampled DFrFT of size N is performed on the aliased time signal. The result of DFrFT is multiplied by the conjugate of the FFT of the local code which is of length L and downsampled by L/N . By performing an inverse sparse Fourier transform (ISFT) to the multiplication result, the aliased time domain output is obtained as

$$s_o(n) = S\mathcal{F}^{-1} \{ \mathcal{F}^\alpha \{ s'(n) \} \cdot C^*(k) \}, \quad (30)$$

where $S\mathcal{F}^{-1}\{\cdot\}$ denotes the ISFT operation.

To determine the unique solution, we first find the bucket with the maximum magnitude among the N buckets; then, we check the correlation of each of the L/N possible time shifts which are aliased into this bucket, and ultimately select the shift that corresponds to the maximum correlation.

Let μ denote the chirp frequency modulation rate, where $\mu = a/\lambda$. From (22) and (28) we know that when $\alpha = \text{arc cot}(-2\pi\mu)$, the chirp signals will focus in the fractional Fourier domain. That is to say, for high dynamic signals, the transform order is relevant to the acceleration of the receiver platform. The relationship between acceleration and transform order is shown in Fig. 7.

B. Algorithm Verification

In this section, the algorithm implementation of high dynamic DSSS signal synchronization is conducted on a GPS navigation platform, which is illustrated in Fig. 8. We first amplify the received satellite signal, and then perform down conversion to the amplified signal, where the adopted IF is 0.42 MHz. After passing through the A/D converter with the sampling rate of 5 MHz, the digitized signals in the two orthogonal inphase (I)

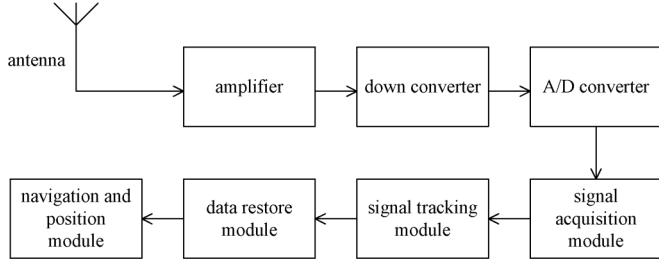


Fig. 8. The architecture of the experimental GPS receiver system.

TABLE I
SIMULATION PARAMETERS

velocity	acceleration	signal length	input SNR
2000 m/s	$60 \times g$	20 ms	-29 dB

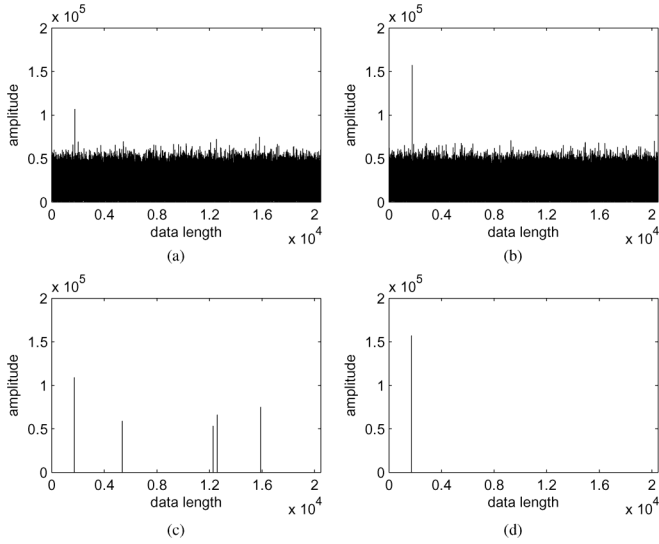


Fig. 9. Simulation results of GPS acquisition using different approaches: (a) FFT. (b) DFrFT. (c) SFT. (d) SDFrFT.

and quadrature (Q) channels are conveyed to the acquisition and tracking module to reconstruct the navigation message.

The following simulation is based on the coarse/acquisition (C/A) code. The C/A code is a pseudo-random (PN) binary sequence, which is transmitted at a rate of 1.023 Mcps/s with the information data rate of 50 bps. The PN sequences only strongly correlate when they are exactly aligned. We choose the L1 wave band as the carrier frequency, whose center frequency is 1575.42 MHz.

The other simulation parameters are listed in Table I. Fig. 9 shows the simulation results using FFT, DFrFT, SFT and SDFrFT. It can be seen that, with the acceleration de-chirped, a more concentrating correlation peak can be obtained by using FrFT approach than by FFT approach. The SDFrFT method only outputs the most significant peak, and the algorithm performs well even in a relatively low SNR environment. By referring to Fig. 3, we draw the conclusion that the proposed method can greatly increase both the probability and the speed of acquisition.

V. SFRCAF AND ITS APPLICATION TO PCL

In this section, we consider another application of the SD-FrFT. The cross ambiguity function (CAF) is a frequently used mathematical tool in radar signal processing, which is used primarily to determine the range and Doppler resolutions of a target in a particular waveform. Other important applications of the CAF embrace estimating the time/frequency difference of arrival at two spatially separated receivers [35] to determine the emitter location and performing coherent integration in a PCL system [36]. Here we mainly focus on its application to the PCL system.

Due to the extraordinary merits of low cost, electromagnetic compatibility, potential anti-stealth capacity and immunity to electronic countermeasures [37], the past few years have witnessed a significant growth of interest and extensive research achievements in the realm of PCL technology. The CAF plays an important role in PCL to increase the signal-to-interference plus noise ratio (SINR) to a detectable level. The corresponding information of targets such as time delay and Doppler shift can be directly obtained from the CAF map [38].

Generally, long time integration is adopted to improve the SINR for weak signals, yet it is accompanied by increased computational complexity. Thus, it is rational that down sampling and the FFT are used to decrease the computation burden, and various versions of CAF are commonly based on this idea [39], [40]. However, in the application scenario where a high frequency resolution is required, the calculation complexity for FFT becomes extremely high because FFT requires $O(N \log_2 N)$ multiplications. In most application situations, nevertheless, only a small number of targets appear in one range cell. Consequently, the CAF plane is dominated by a small number of peaks, namely, a sparse feature is presented. In this case, we propose a novel SFrCAF algorithm based on the SDFrFT to promote the operation efficiency.

A. Principle

In this section, the definition and the derivation of the novel SFrCAF are discussed in a PCL radar scenario.

A PCL system utilizes the direct wave signal and the target echo signal to calculate CAF. The CAF is calculated as

$$|\Psi(\tau, f_d)| = \left| \int_0^{T_{\text{int}}} s_e(t + \tau) s_r^*(t) e^{-j2\pi f_d t} dt \right|, \quad (31)$$

where $s_e(t)$ is the echo signal received by the surveillance antenna, $s_r(t)$ is the direct path signal received by the reference antenna, τ and f_d denote the time delay and the Doppler shift, respectively, and T_{int} is the integration time. It is worth noting that the CAF in (31) can be interpreted as the Fourier transform of the product of the delayed version of $s_e(t)$ and the conjugate of $s_r(t)$.

The discrete definition of CAF can be written as follows:

$$\Psi(d, q) = \sum_{n=0}^{L-1} s_e(n+d) \cdot s_r^*(n) \cdot e^{-j\frac{2\pi}{T} nq}, \quad (32)$$

where $s_e(n)$ and $s_r(n)$ are the sampled echo and reference signals, respectively. In addition, d is the number of delay bins, q is the number of Doppler shift bins, and L refers to the integration length of data. Then, the integration time of CAF is

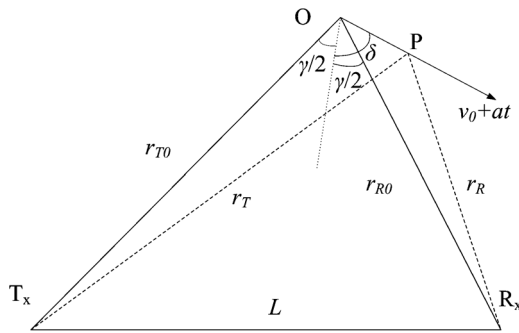


Fig. 10. The bistatic geometry of PCL.

$T_{\text{int}} = L \cdot \Delta t$. By adopting low-pass filtering and M times down sampling to the product of $s_e(n+d) \cdot s_r^*(n)$, we can obtain $x(d, n)$, where $n \in [1, N]$, and the number of integration points is $N = L/M$. Then, the calculation of (32) can be simplified as

$$\Psi(d, q) = \text{FFT} \{x(d, n)\}. \quad (33)$$

After down sampling, the frequency domain observation range is $[-f_s/(2M), f_s/(2M)]$, where $f_s = 1/\Delta t$ denotes the base-band sampling rate.

In practice, when the frequency spectrum of the targets is sparse, the FFT can be replaced by the SDFrFT in the calculation of the CAF to improve the operation efficiency.

When a target with accelerating motion is to be detected, the Doppler migration should be considered. The bistatic configuration of PCL is illustrated in Fig. 10, where T_x and R_x denote the location of the non-cooperative transmitter and the receiver, respectively. At the initial time, the target is located at O , accelerating with the initial velocity v_0 and a constant acceleration a along the straight line which slants at an angle of δ to the bistatic angular bisector. The bistatic angular is γ , and L denotes the baseline distance. At time t , it reaches the location P . r_{T0} , $r_T(t)$, r_{R0} and $r_R(t)$ represent the distance between the target and the transmitter or the receiver at the initial time or at t , respectively.

From Fig. 10, we can obtain the bistatic range as (34), shown at the bottom of the page. Let c be the velocity of light. The bistatic time delay and Doppler frequency can be derived from (35) and (36), respectively, and expressed as

$$\tau(t) = \frac{r(t) - L}{c}, \quad (35)$$

$$f_d(t) = -\frac{1}{\lambda} \frac{dr(t)}{dt}. \quad (36)$$

Substituting (34) into (35) and (36), then performing Taylor series expansion at $t = 0$ with the quadratic and higher terms neglected, we can get

$$\tau(t) \triangleq \tau_0 + a_\tau t \approx \frac{r_{T0} + r_{R0} - L}{c} + \frac{-2v_0 \cos \delta \cos \frac{\gamma}{2}}{c} t, \quad (37)$$

$$f_d(t) \triangleq f_{d0} + \mu t \approx \frac{2v_0}{\lambda} \cos \delta \cos \frac{\gamma}{2} + \frac{1}{\lambda} \left(2a \cos \delta \cos \frac{\gamma}{2} - \frac{v_0^2 \sin^2 \left(\delta + \frac{\gamma}{2} \right)}{r_{T0}} - \frac{v_0^2 \sin^2 \left(\delta - \frac{\gamma}{2} \right)}{r_{R0}} \right) t. \quad (38)$$

Therefore, the relationship between the echo signal and the direct path signal can be written as

$$s_e(t) = A_0 s_r(t - \tau_0 - a_\tau t) e^{j2\pi f_{d0} t} e^{j\pi \mu t^2}, \quad (39)$$

where A_0 represents the amplitude of the echo signal. Note that (39) describes an ideal model of the relationship between the received signals, which is derived from the scenario illustrated in Fig. 10 with a single target, which undergoes maneuvering with a constant acceleration within the integration time. As we pointed out prior to (37) and (38), the quadratic and higher terms are neglected. Empirical knowledge and studies in other literatures [41], [42] reveal that the simplified model is sufficient for theoretical discussion and practical applications.

In this case, DFrFT is an effective measure to compensate the Doppler migration so as to improve the SINR. Comparing (31) and (39) with (22), we can see that, to reach the best compensation performance, the rotation angle α needs to satisfy

$$\alpha = \text{arc cot}(-2\pi\mu) = \text{arc cot} \left(\frac{-2\pi}{\lambda} \left(2a \cos \delta \cos \frac{\gamma}{2} - \frac{v_0^2 \sin^2 \left(\delta + \frac{\gamma}{2} \right)}{r_{T0}} - \frac{v_0^2 \sin^2 \left(\delta - \frac{\gamma}{2} \right)}{r_{R0}} \right) \right). \quad (40)$$

At this point, the time delay, the Doppler frequency and the acceleration of a certain target can be estimated by the α -order FrCAF as

$$\begin{aligned} (\hat{\tau}, \hat{f}_d, \hat{\mu}) &= \arg \max_{\tau, f_d, \mu} |\Psi^\alpha(\tau, f_d, \mu)| \\ &= \arg \max_{\tau, f_d, \mu} \left| \mathcal{F}^\alpha \left\{ x \left(\frac{\tau}{\Delta t}, n \right) \right\} \right|. \end{aligned} \quad (41)$$

$$\begin{aligned} r(t) &= r_T(t) + r_R(t) \\ &= \sqrt{r_{T0}^2 + \left(\int_0^t (v_0 + at) dt \right)^2} - 2r_{T0} \left(\int_0^t (v_0 + at) dt \right) \cos \left(\delta + \frac{\gamma}{2} \right) \\ &\quad + \sqrt{r_{R0}^2 + \left(\int_0^t (v_0 + at) dt \right)^2} - 2r_{R0} \left(\int_0^t (v_0 + at) dt \right) \cos \left(\delta - \frac{\gamma}{2} \right). \end{aligned} \quad (34)$$

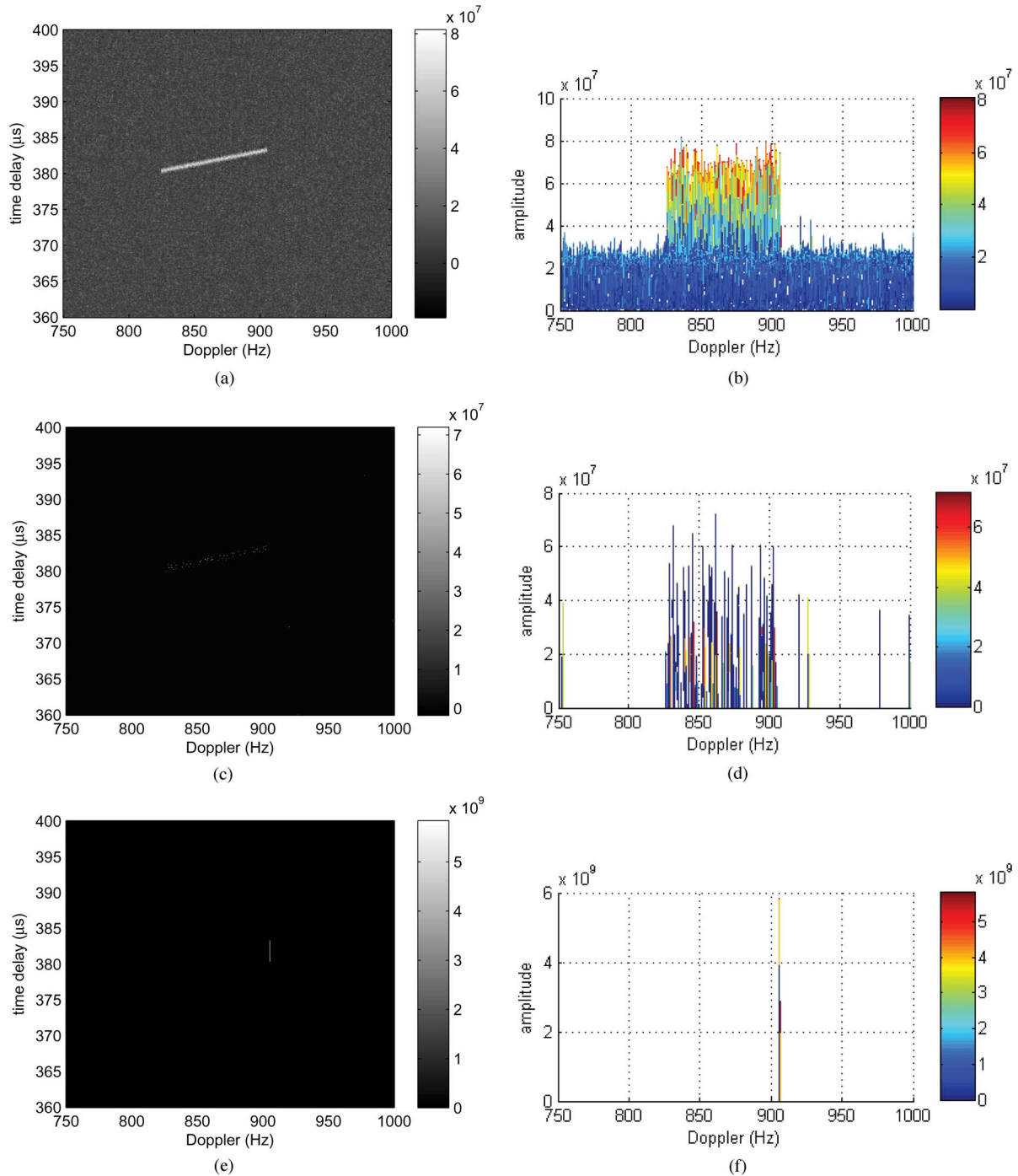


Fig. 11. Simulation results of coherent integration using different approaches: (a) CAF result with FFT. (b) Side view of Doppler-amplitude section of the CAF map in (a). (c) SFrCAF result with SFT, namely $\alpha = 0$. (d) Side view of Doppler-amplitude section of the SFrCAF map in (c). (e) SFrCAF result, where Doppler migration has been compensated at $\alpha = 0.0080$ rad. (f) Side view of Doppler-amplitude section of the SFrCAF map in (e).

For the additional dimension to the conventional CAF, the FrCAF is more time-consuming, and thus greatly limits its application range. By adopting the proposed SDFrFT based method, a significant reduction in the overall runtime can be achieved. Thus, the proposed α -order SFrCAF can be expressed as

$$S\Psi^\alpha(d, q) = \{S\mathcal{F}^\alpha x\}(d, n), \quad (42)$$

where $\{S\mathcal{F}^\alpha x\}(d, n)$ denotes the α -order SDFrFT operation to signal $x(d, n)$.

In the case where *a priori* information suggests that the target remains in its state of radial uniform motion during the integration time, the SDFrFT process can be further simplified to the SFT.

B. Algorithm Verification

The aforementioned algorithm is validated by the following simulation and real data experiment, where the digital video broadcast signal is adopted as the non-cooperative transmitted

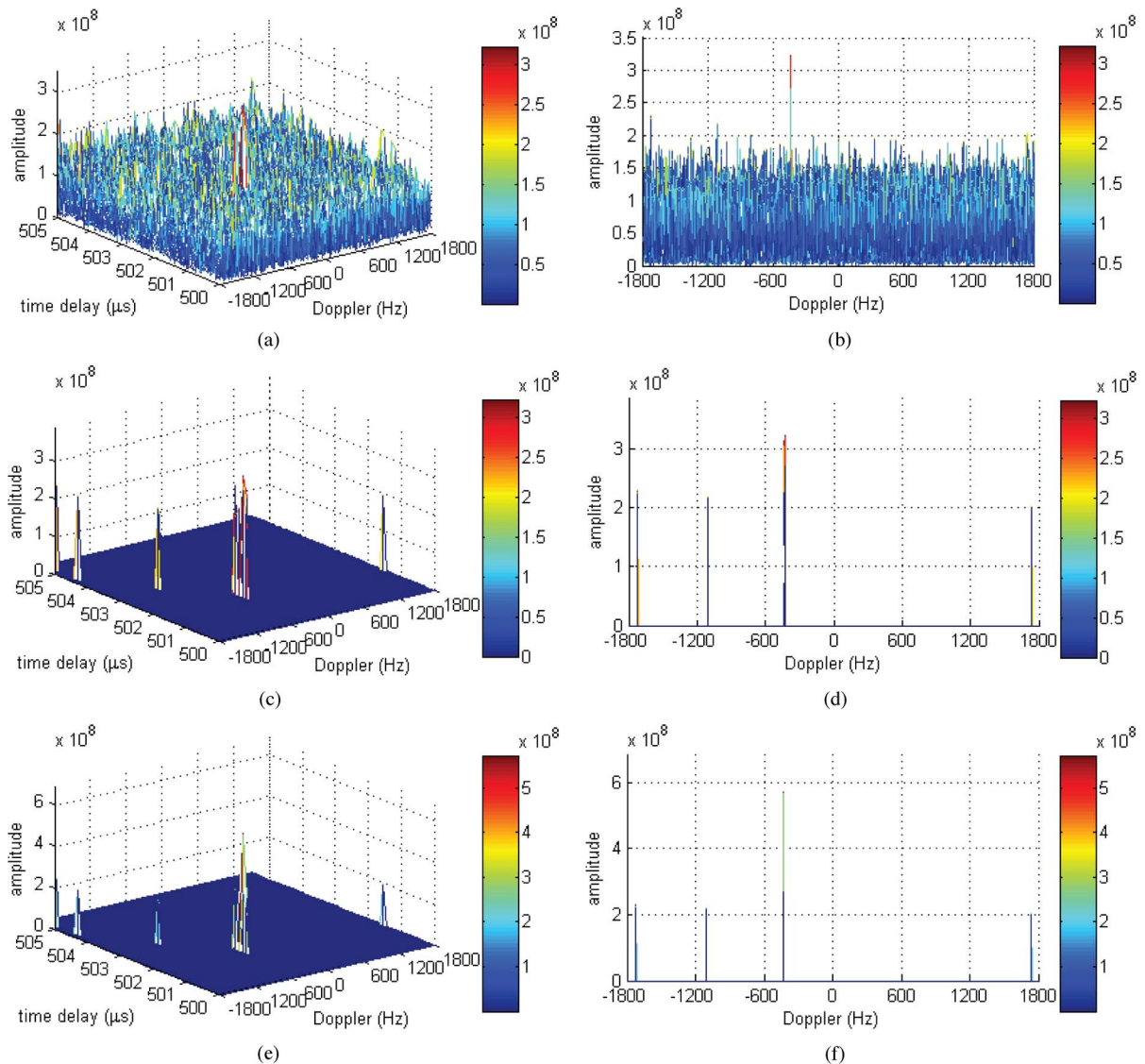


Fig. 12. Real data experiment results of coherent integration using different approaches: (a) CAF result of real data. (b) Side view of Doppler-amplitude section of the CAF map in (a). (c) SFrCAF result with SFT, namely $\alpha = 0$. (d) Side view of Doppler-amplitude section of the SFrCAF map in (c). (e) SFrCAF result of real data, where $\alpha = 0.0681$ rad. (f) Side view of Doppler-amplitude section of the SFrCAF map in (e).

TABLE II
TARGET PARAMETERS OF THE TARGET WITH ACCELERATING MOTION

r_{T0}	r_{R0}	L	γ
175 km	120 km	180 km	72.5°
v_0	a	FFT points	downsampling rate
250 m/s	-10 m/s ²	16384	1200

signal. The bandwidth B , the carrier frequency f_c and the base-band sampling rate f_s are 7.56 MHz, 674 MHz and 9 MHz, respectively.

1) *Simulation: Detection of Target With Accelerating Motion*: In the simulation, the other corresponding parameters of the accelerating target are as listed in Table II. The target uniformly accelerates along the bistatic angular bisector with the initial velocity v_0 and acceleration a . Figs. 11(a) and (b) show the CAF results using FFT, where the Doppler migration is highly conspicuous, thus the energy of the target echo does not focus in a single frequency bin. By adopting the SFrCAF

of the same data length, when α is rotated to an appropriate angle, the Doppler migration is compensated, which is shown in Figs. 11(e) and (f), while the runtime is dramatically decreased. According to (41), with the optimum rotation angle α and the location of the delay/Doppler bin, we can estimate the bistatic acceleration, range and velocity of the target.

Note that an obvious range migration can be observed in the simulation result depicted in Fig. 11(e). However, the Keystone transform based solution to this problem has been well established in our previous work [41]. We do not discuss it here for conciseness since it is out of the scope of this paper.

2) *Real Offline Data Experiment*: In this example, we use a real recorded experiment data set to conduct the offline signal processing. The processed results of the CAF and the SFrCAF are shown in Fig. 12. The length of the data to be processed is 3932160 samples, which is downsampled by a rate of 120 before performing coherent integration. In the SFrCAF processing, the optimum rotation angle is estimated as $\alpha = 0.0681$ rad. The bistatic Doppler frequency, the time delay, and the variation rate

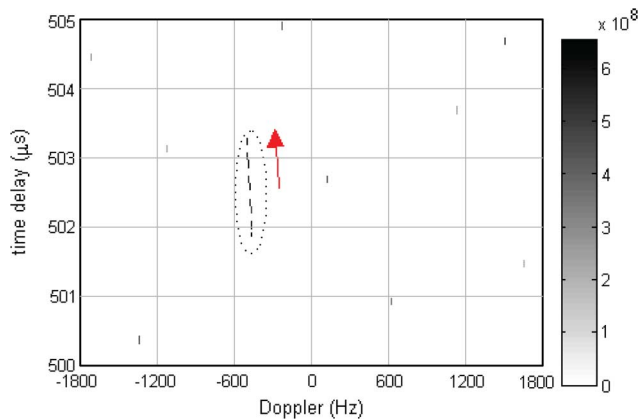


Fig. 13. Superposition of detection results over data files sequence.

of the bistatic velocity are estimated as -437.2 Hz, 501.8 μ s, and -2.3335 m/s^2 , respectively.

The effectiveness of the proposed SFrCAF is verified by the performance as shown in Fig. 12, where the motion parameters of the target are accurately estimated by SDFrFT, and a fine detection performance is achieved with a notably reduced computational complexity. By comparing the algorithm performances shown in Figs. 12(d) and (f), the target's amplitude in Fig. 12(f) is approximately 4.9 dB higher than that in Fig. 12(d). Therefore, we can conclude that the peak energy of the accelerating target is more concentrated with SDFrFT than with SFT, so that the target can be better distinguished from interference. It is rational to predict that in CAF application, the advantage of SDFrFT over SFT will be more pronounced when the acceleration is higher.

In the following, we further demonstrate target detection over multiple coherent processing intervals by performing SFrCAF on a sequence of 9 consecutive data files. The length of each data file is 0.5 s, i.e., 4.5×10^6 samples, in which the first 3932160 samples are utilized. Then we draw the superposition of the processing results over these data files plotted in Fig. 13, yielding the trajectory of the target that moves away from the radar. In particular, the interval between the neighboring trace points matches the product of the target Doppler and the length of data file, and the changing rate of the Doppler frequency also matches the estimated acceleration. On the other hand, other non-target components randomly scatter on the CAF surface, and no connection between them can be observed. The offline data detection results have also been compared against the recorded log of the ADS-B receiver in our experimental data acquisition system to verify their consistency with the ground truth. As such, through the superposition of the consecutive processing results, we are able to clearly identify and track a weak target in the presence of other strong echo components.

To summarize, the proposed SFrCAF is applicable to the detection scenarios where the data length is sufficiently large and the radial acceleration remains roughly stable during the integration time. When SFrCAF is adopted, a relatively higher integration gain can be obtained with a faster acceleration rate of the target, and an accelerated algorithm computation can be achieved with a larger data length. From the implementation perspective, the inherent data-parallelism of the proposed SFrCAF, which is embodied in the computing patterns of

location/estimation loops and Doppler filtering at different time delays, may facilitate its efficient realization on a programmable graphic processing unit (GPU) via NVidia's compute unified device architecture (CUDA) paradigm, thus GPU could be a preferred selection in practice.

VI. CONCLUSION

The objective of this paper was to develop a numerical algorithm for the fast computation of DFrFT when the signal spectrum can be sparsely represented in the fractional Fourier domain. By recurring to the merit of SFT, we have redesigned the Pei's algorithm and proposed a novel approach, which significantly outperforms the existing algorithms in the runtime aspect. The application of the proposed SDFrFT algorithm for the fast synchronization of the high dynamic DSSS signal was then presented. We have also proposed a SFrCAF for radar signal processing and applied it to the coherent integration in a PCL system. The simulation results clearly demonstrated the applicability of the proposed algorithm to the fast analysis of non-stationary signals with a large size and sparse spectrum in the fractional Fourier domain. Our future work will concentrate on further optimizing the algorithm, and generalizing the method to the case of the discrete linear canonical transform.

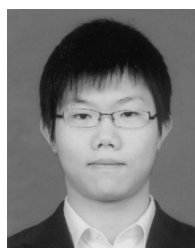
ACKNOWLEDGMENT

The authors would like to thank the anonymous reviewers for their valuable comments, which have helped improve the quality and clarity of this paper. Tao Shan would also like to thank the China Scholarship Council for support.

REFERENCES

- [1] S. C. Pei and W. L. Hsue, "Random discrete fractional Fourier transform," *IEEE Signal Process. Lett.*, vol. 16, no. 12, pp. 1015–1018, Dec. 2009.
- [2] J. W. Cooley and J. W. Tukey, "An algorithm for the machine computation of complex Fourier series," *Math. Comput.*, vol. 19, no. 90, pp. 297–301, Apr. 1965.
- [3] S. C. Pei, C. C. Tseng, and M. H. Yeh, "A new discrete fractional Fourier transform based on constrained eigendecomposition of DFT matrix by Lagrange multiplier method," *IEEE Trans. Circuits Syst. II, Analog Digit. Signal Process.*, vol. 46, no. 9, pp. 1240–1245, Sep. 1999.
- [4] C. Candan, M. A. Kutay, and H. M. Ozaktas, "The discrete fractional Fourier transform," *IEEE Trans. Signal Process.*, vol. 48, no. 5, pp. 1329–1337, May 2000.
- [5] M. T. Hanna, "Fractional discrete Fourier transform of type IV based on the eigenanalysis of a nearly tridiagonal matrix," *Digit. Signal Process.*, vol. 22, no. 6, pp. 1095–1106, Dec. 2012.
- [6] B. Santhanam and J. H. McClellan, "The discrete rotational Fourier transform," *IEEE Trans. Signal Process.*, vol. 44, no. 4, pp. 994–998, Apr. 1996.
- [7] T. Erseghe, P. Kraniuskas, and G. Cariolaro, "Unified fractional Fourier transform and sampling theorem," *IEEE Trans. Signal Process.*, vol. 47, no. 12, pp. 3419–3423, Dec. 1999.
- [8] H. M. Ozaktas, O. Ankan, M. A. Kutay, and G. Bozdagt, "Digital computation of the fractional Fourier transform," *IEEE Trans. Signal Process.*, vol. 44, no. 9, pp. 2141–2150, Sep. 1996.
- [9] S. C. Pei and J. J. Ding, "Closed-form discrete fractional and affine Fourier transforms," *IEEE Trans. Signal Process.*, vol. 48, no. 5, pp. 1338–1353, May 2000.
- [10] H. Hassanieh, P. Indyk, D. Katabi, and E. Price, "Simple and practical algorithm for sparse Fourier transform," in *Proc. 23rd Annu. ACM-SIAM Symp. Discrete Algorithms*, Kyoto, Japan, Jan. 2012, pp. 1183–1194.

- [11] A. C. Gilbert, P. Indyk, M. Iwen, and L. Schmidt, "Recent developments in the sparse Fourier transform: A compressed Fourier transform for big data," *IEEE Signal Process. Mag.*, vol. 31, no. 5, pp. 91–100, Sep. 2014.
- [12] J. Markel, "FFT pruning," *IEEE Trans. Audio Electroacoust.*, vol. 19, no. 4, pp. 305–311, Dec. 1971.
- [13] R. Tao, B. Z. Li, and Y. Wang, "Spectral analysis and reconstruction for periodic nonuniformly sampled signals in fractional Fourier domain," *IEEE Trans. Signal Process.*, vol. 55, no. 7, pp. 3541–3547, Jul. 2007.
- [14] R. Tao, F. Zhang, and Y. Wang, "Fractional power spectrum," *IEEE Trans. Signal Process.*, vol. 56, no. 9, pp. 4199–4206, Sep. 2008.
- [15] R. Tao, B. Deng, W. Q. Zhang, and Y. Wang, "Sampling and sampling rate conversion of band limited signals in the fractional Fourier transform domain," *IEEE Trans. Signal Process.*, vol. 56, no. 1, pp. 158–171, Jan. 2008.
- [16] R. Tao, F. Zhang, and Y. Wang, "Sampling random signals in a fractional Fourier domain," *Signal Process.*, vol. 91, no. 6, pp. 1394–1400, Jun. 2011.
- [17] R. Tao, X. M. Li, Y. L. Li, and Y. Wang, "Time delay estimation of chirp signals in the fractional Fourier domain," *IEEE Trans. Signal Process.*, vol. 57, no. 7, pp. 2852–2855, Jul. 2009.
- [18] R. Tao, Y. L. Li, and Y. Wang, "Short-time fractional Fourier transform and its applications," *IEEE Trans. Signal Process.*, vol. 58, no. 5, pp. 2568–2580, May 2010.
- [19] E. Sejdic, I. Djurovic, and L. Stankovic, "Fractional Fourier transform as a signal processing tool: An overview of recent developments," *Signal Process.*, vol. 91, no. 6, pp. 1351–1369, June 2011.
- [20] A. Omid, H. Ezz, H. Haitham, A. Abhinav, K. Dina, C. P. Anantha, and S. Vladimir, "A 0.75-million-point fourier-transform chip for frequency-sparse signals," in *IEEE Int. Solid-State Circuits Conf. Dig. Tech. Papers (ISSCC)*, San Francisco, CA, USA, Feb. 2014, pp. 458–459.
- [21] J. Schumacher, "High performance sparse fast Fourier transform," M.S. thesis, ETH Zurich, Zurich, Switzerland, 2013.
- [22] S. Peleg and B. Friedlander, "The discrete polynomial-phase transform," *IEEE Trans. Signal Process.*, vol. 43, no. 8, pp. 1901–1914, Aug. 1995.
- [23] S. Peleg and B. Friedlander, "Multicomponent signal analysis using the polynomial-phase transform," *IEEE Trans. Aerosp. Electron. Syst.*, vol. 32, no. 1, pp. 378–387, Jan. 1996.
- [24] T. Abotzoglou, "Fast maximum likelihood joint estimation of frequency and frequency rate," *IEEE Trans. Acoust., Speech Signal Process.*, vol. 22, no. 6, pp. 708–715, Jun. 1986.
- [25] X. G. Xia, "Discrete chirp-Fourier transform and its application to chirp rate estimation," *IEEE Trans. Signal Process.*, vol. 48, no. 11, pp. 3122–3133, Nov. 2000.
- [26] P. M. Djuric and S. M. Kay, "Parameter estimation of chirp signals," *IEEE Trans. Signal Process.*, vol. 38, no. 12, pp. 2118–2126, Dec. 1990.
- [27] L. B. Almeida, "The fractional Fourier transform and time-frequency representations," *IEEE Trans. Signal Process.*, vol. 42, no. 11, pp. 3084–3091, Nov. 1994.
- [28] L. B. Almeida, Dec. 2013, The Code sFFT-1.0–2.0 Package [Online]. Available: <http://groups.csail.mit.edu/netmit/sFFT/sFFT-1.0-2.0.tar.gz>
- [29] H. Hassanieh, P. Indyk, D. Katabi, and E. Price, "Nearly optimal sparse Fourier transform," in *Proc. 44th Symp. Theory Comput.*, New York, NY, USA, Jan. 2012, pp. 563–578.
- [30] A. J. Viterbi, *CDMA Principles of Spread Spectrum Communication*. Reading, MA, USA: Addison-Wesley, 1995.
- [31] B. Hofmann-Wellenhof, H. Lichtenegger, and J. Collins, *Global Positioning System: Theory and Practice*. Vienna, Italy: Springer, 1993.
- [32] S. M. Spangenberg, I. Scott, S. McLaughlin, G. J. Povey, D. G. Cruickshank, and P. M. Grant, "An FFT-based approach for fast acquisition in spread spectrum communication systems," *Wireless Pers. Commun.*, vol. 13, no. 1–2, pp. 27–55, May 2000.
- [33] D. Akopian, "Fast FFT based GPS satellite acquisition methods," *Proc. Inst. Electr. Eng.—Radar Sonar Navig.*, vol. 152, no. 4, pp. 277–286, Aug. 2005.
- [34] H. Hassanieh, F. Adib, D. Katabi, and P. Indyk, "Faster GPS via the sparse Fourier transform," in *Proc. ACM MobiCom*, Istanbul, Turkey, Aug. 2012, pp. 353–364.
- [35] K. P. Bentz, "Computation of the cross ambiguity function using perfect reconstruction DFT filter banks," Ph.D. dissertation, George Mason Univ., Fairfax, VA, USA, 2007.
- [36] J. E. Palmer, H. A. Harms, S. J. Searle, and L. M. Davis, "DVB-T passive radar signal processing," *IEEE Trans. Signal Process.*, vol. 61, no. 8, pp. 2116–2126, Apr. 2013.
- [37] H. D. Griffiths and C. J. Baker, "Passive coherent location radar systems. Part 1: Performance prediction," *Proc. Inst. Electr. Eng.—Radar Sonar Navig.*, vol. 152, no. 3, pp. 153–159, Jun. 2005.
- [38] H. D. Griffiths, C. J. Baker, H. Ghaleb, R. Ramakrishnan, and E. Willman, "Measurement and analysis of ambiguity functions of off-air signals for passive coherent location," *Electron. Lett.*, vol. 39, no. 13, pp. 1005–1007, Jun. 2003.
- [39] R. Tolimieri and S. Winograd, "Computing the ambiguity surface," *IEEE Trans. Acoust., Speech, Signal Process.*, vol. 33, no. 5, pp. 1239–1245, May 1985.
- [40] C. L. Yatrakis, "Computing the cross-ambiguity function—A review," B.S. thesis, State Univ. of New York, Binghamton, NY, USA, 2005.
- [41] Y. Feng, T. Shan, Z. H. Zhuo, and R. Tao, "The migration compensation methods for DTV based passive radar," in *Proc. IEEE Radar Conf.*, Ottawa, ON, Canada, May 2013, pp. 1–4.
- [42] D. W. O'Hagan, H. Kuschel, M. Ummerhofer, J. Heckenbach, and J. Schell, "A multi-frequency hybrid passive radar concept for medium range air surveillance," *IEEE Aerosp. Electron. Syst. Mag.*, vol. 27, no. 10, pp. 6–15, Oct. 2012.



Shengheng Liu (S'14) was born in 1987. He was admitted to the Ph.D. program directly from B.S. degree, exempting from the qualification examination in the year 2010 for his exceptional performance during undergraduate years in Beijing Institute of Technology, and he is currently working toward the Ph.D. degree. His research interests include fractional Fourier transform and passive bistatic radar signal processing.



Tao Shan was born in 1969. He received his B.S. degree from Xidian University, Xi'an, in 1991 and Ph.D. degree from Beijing Institute of Technology in 2004. He is an associate professor with the School of Information and Electronics, Beijing Institute of Technology. Currently, he is a visiting scholar at the Center for Advanced Communications, Villanova University. He was a recipient of the first prize of science and technology progress awarded by the Ministry of Education in 2006 and 2007 respectively. His research interests include radar signal processing and complex information system theory.



Ran Tao (M'00–SM'04) was born in 1964. He received the B.S. degree from Electronic Engineering Institute of PLA, Hefei, in 1985 and the M.S. and Ph.D. degrees from Harbin Institute of Technology, Harbin, in 1990 and 1993, respectively. In 2001, he was a senior visiting scholar in the University of Michigan, Ann Arbor. He is currently a Professor with the School of Information and Electronics, Beijing Institute of Technology, Beijing, China. He was a recipient of National Science Foundation of China for Distinguished Young Scholars in 2006,

and a Distinguished Professor of Changjiang Scholars Program in 2009. He has been a Chief Professor of the Creative Research Groups of the National Natural Science Foundation of China since 2014, and he was a Chief Professor of the Program for Changjiang Scholars and Innovative Research Team in University during 2010 to 2012. He is currently the Vice Chair of IEEE China Council. He is also the Vice Chair of the International Union of Radio Science (URSI) China Council and a Member of Wireless Communication and Signal

Processing Commission of URSI. He was a recipient of the first prize of science and technology progress in 2006, 2007, respectively, and the first prize of natural science in 2013, both awarded by the Ministry of Education. His current research interests include fractional Fourier transform and its applications, theory and technology for radar and communication systems. He has 3 books and more than 100 peer-reviewed journal articles.



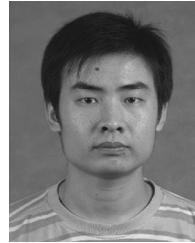
Yimin D. Zhang (SM'01) received his Ph.D. degree from the University of Tsukuba, Tsukuba, Japan, in 1988.

He joined the faculty of the Department of Radio Engineering, Southeast University, Nanjing, China, in 1988. He served as a Director and Technical Manager at the Oriental Science Laboratory, Yokohama, Japan, from 1989 to 1995, and a Senior Technical Manager at the Communication Laboratory Japan, Kawasaki, Japan, from 1995 to 1997. He was a Visiting Researcher at the ATR Adaptive Communications Research Laboratories, Kyoto, Japan, from 1997 to 1998. Since 1998, he has been with the Villanova University, Villanova, PA, where he is currently a Research Professor with the Center for Advanced Communications, and is the Director of the Wireless Communications and Positioning Laboratory and the Director of the Radio Frequency Identification (RFID) Laboratory. His general research interests lie in the areas of statistical signal and array processing for radar, communications, and navigation applications, including compressive sensing, convex optimization, nonstationary signal and time-frequency analysis, MIMO systems, radar imaging, target localization and tracking, wireless and cooperative networks, and jammer suppression. He has 11 book chapters and more than 200 journal articles and peer-reviewed conference papers.

Dr. Zhang serves on the Editorial Board of the *Signal Processing* journal. He was an Associate Editor for the IEEE TRANSACTIONS ON SIGNAL PROCESSING during 2010–2014, an Associate Editor for the IEEE SIGNAL PROCESSING LETTERS during 2006–2010, and an Associate Editor for the *Journal of the Franklin Institute* during 2007–2013. He is a Technical Committee Co-chair of the IEEE Benjamin Franklin Symposium on Microwave and Antenna Sub-systems in 2014 and 2015.



Guo Zhang was born in 1989. She received her B.S. and M.S. degree from Beijing Institute of Technology in 2011 and 2014, respectively. She is currently with Beijing Telecom Planning & Designing Institute Co., Ltd. Her research interest is radar signal processing.



Feng Zhang (M'10) was born in 1981. He received his B.S. and M.S. degrees from Zhengzhou University, Zhengzhou, in 2003 and 2006, respectively, and Ph.D. degree from Beijing Institute of Technology in 2010. Now he is an associate professor with the School of Information and Electronics, Beijing Institute of Technology. He was a recipient of the first prize of natural science awarded by the Ministry of Education in 2013. His research interests include time-frequency analysis, digital image processing, fractional Fourier transform, and

multirate signal processing.



Yue Wang was born in 1932. He received the B.S. degree from Xidian University, Xi'an, in 1956. He is an academican of both Chinese Academy of Science and Chinese Academy of Engineering. He was the president of Beijing Institute of Technology from 1993 to 1999. He is currently a professor with Beijing Institute of Technology. His research interests are complex system theory, radar signal processing and information countermeasures.